

Article

Carcinoma-Associated Mesenchymal Stem Cells Promote Chemoresistance in Ovarian Cancer Stem Cells via PDGF Signaling

Shreya Raghavan ^{1,†} , Catherine S. Snyder ^{1,†} , Anni Wang ^{2,†}, Karen McLean ^{3,4} ,
Dmitriy Zamarin ⁵, Ronald J. Buckanovich ⁶ and Geeta Mehta ^{1,2,4,7,8,*} 

¹ Department of Materials Science and Engineering, University of Michigan, Ann Arbor, MI 48109, USA; shreyar@umich.edu (S.R.); cssnyder@umich.edu (C.S.S.)

² Department of Biomedical Engineering, University of Michigan, Ann Arbor, MI 48109, USA; anniwang@umich.edu

³ Department of Obstetrics and Gynecology, Division of Gynecologic Oncology, Michigan Medicine, University of Michigan, Ann Arbor, MI 48109, USA; karenmcl@umich.edu

⁴ Rogel Cancer Center, University of Michigan, Ann Arbor, MI 48109, USA

⁵ Department of Gynecologic Medical Oncology and Immunotherapeutics, Memorial Sloan Kettering Cancer Center, New York, NY 10065, USA; zamarind@mskcc.org

⁶ Director of Ovarian Cancer Research, Magee Womens Research Institute, University of Pittsburgh, Pittsburgh, PA 15260, USA; buckanovichrj@mwri.magee.edu

⁷ Department of Macromolecular Sciences and Engineering, University of Michigan, Ann Arbor, MI 48109, USA

⁸ Precision Health, University of Michigan, Ann Arbor, MI 48109, USA

* Correspondence: mehtagee@umich.edu; Tel.: +1-734-763-3957; Fax: +1-734-763-4788

† These authors contributed equally to this work.

Received: 28 June 2020; Accepted: 23 July 2020; Published: 27 July 2020



Abstract: Within the ovarian cancer tumor microenvironment, cancer stem-like cells (CSC) interact with carcinoma associated mesenchymal stem/stromal cells (CA-MSC) through multiple secreted cytokines and growth factors. These paracrine interactions have been revealed to cause enrichment of CSC and their chemoprotection; however, it is still not known if platelet-derived growth factor (PDGF) signaling is involved in facilitating these responses. In order to probe this undiscovered bidirectional communication, we created a model of ovarian malignant ascites in the three-dimensional (3D) hanging drop heterospheroid array, with CSC and CA-MSC. We hypothesized that PDGF secretion by CA-MSC increases self-renewal, migration, epithelial to mesenchymal transition (EMT) and chemoresistance in ovarian CSC. Our results indicate that PDGF signaling in the CSC-MSC heterospheroids significantly increased stemness, metastatic potential and chemoresistance of CSC. Knockdown of *PDGFB* in MSC resulted in abrogation of these phenotypes in the heterospheroids. Our studies also reveal a cross-talk between PDGF and Hedgehog signaling in ovarian cancer. Overall, our data suggest that when the stromal signaling via PDGF to ovarian CSC is blocked in addition to chemotherapy pressure, the tumor cells are significantly more sensitive to chemotherapy. Our results emphasize the importance of disrupting the signals from the microenvironment to the tumor cells, in order to improve response rates. These findings may lead to the development of combination therapies targeting stromal signaling (such as PDGF and Hedgehog) that can abrogate the tumorigenic, metastatic and platinum resistant phenotypes of ovarian CSC through additional investigations.

Keywords: ovarian cancer; cancer stem-like cells (CSC); carcinoma associated mesenchymal stem cells (CA-MSC); platelet derived growth factor (PDGF); stemness; chemoresistance; high grade serous ovarian cancers; 3D spheroids; tumoroids; heterospheroids; stromal cells

1. Introduction

Ovarian cancer is the fifth leading cause of cancer-related deaths in women in the United States, and has a low survival rate, due in part to the frequent late stage at diagnosis [1,2]. Despite aggressive surgical debulking and first-line platinum-based therapy, a ~70% relapse rate is observed, attributable to chemoresistance and peritoneal metastasis [1]. Chemoresistance and new tumor growth following primary therapy has been ascribed to ovarian cancer stem cells (CSC), through a complex interplay with other cells within the tumor microenvironment (TME) [1,3–7]. Previous studies have indicated that CSC in ovarian cancer are identified with high CD133 expression and increased aldehyde dehydrogenases (ALDH) activity, and presence of these cells predicts prognosis for reduced progression-free survival and poor patient outcome [8–21]. Additionally, elevated ALDH activity alone has been utilized in previous studies as a marker of the CSC progenies [8–21].

Stromal cells within the TME, including carcinoma-associated mesenchymal stem/stromal cells (CA-MSC) play critical supportive roles aiding in CSC proliferation, metastasis and chemoresistance [22–25]. CA-MSC arise from tumor mediated reprogramming of local tissue MSC, and have been linked to increased tumorigenesis and chemoresistance through secretion of a complex cytokine network involving IL-6, SDF-1, TGF- β , BMP2, BMP4 and CCL5 [22,23,26–28]. Co-culture of ovarian cancer cells with MSC leads to increased proliferation, invasiveness and platinum resistance of the cancer cells [29,30]. Additionally, ovarian CSC and CA-MSC are known to communicate bi-directionally, with CSCs possessing the ability to impact the phenotype of MSCs to make them more tumor-supportive [26]. Within the framework of this dynamic CSC/CA-MSC relationship, we hypothesize that platelet-derived growth factor (PDGF) plays a critical role in CSC/CA-MSC pro-tumorigenic signaling.

The PDGF family has been shown to play a crucial role in MSC differentiation and growth [31] and can protect MSC from apoptosis and senescence [32]. Additionally, in ovarian cancers, PDGF ligands, including PDGF-BB, and their corresponding receptors (PDGFR) have been noted as a potential key pathway with poor prognosis, yet PDGF signaling is poorly studied in the context of ovarian CSC/CA-MSC interactions [33–36]. PDGFR are known to promote CSC phenotypes in sarcomas [37]. PDGF signaling has also been linked to the formation and maintenance of glioma, gastric cancer, lung cancer and breast cancer, among others [38–43]. Downstream of the PDGF-BB/PDGFR interaction, several mechanistic pathways have been shown to increase tumorigenicity, metastasis and CSC phenotypes. Among those documented are the epithelial to mesenchymal transition (EMT) pathway in several cancers, as well as the Hedgehog (HH) signaling pathway [44–47]. Importantly, the multitargeted tyrosine kinase inhibitor, sunitinib and Hedgehog signaling pathway (Smoothed) inhibitor, sonidegib, have been explored in randomized phase II settings, demonstrating moderate single agent efficacy in targeting stromal components in ovarian and other cancers [48–54].

In this study, we utilized a three-dimensional (3D) hanging drop array spheroid platform, to bring CSC and human adipose MSC (MSC) or carcinoma-associated primary MSC (CA-MSC) in close association in a non-adherent 3D in vitro structure, similar to their presence and interactions within the malignant ascites [19,50,55–58]. Using this model, we aimed to investigate the hypothesized PDGF-BB/PDGFR- β signaling and its downstream effects on functional CSC behaviors, including migratory potential, tumorigenicity and platinum resistance. In addition, we evaluated the role of PDGF-BB/PDGFR- β interactions in promoting EMT and/or Hedgehog signaling, and their effect on the metastatic and tumorigenic CSC phenotype. Overall, coupled with the importance of PDGF as a prognostic marker for ovarian cancer, we believe that disrupting the trophic signaling between CA-MSC and CSC by inhibiting PDGF signaling is a novel therapeutic avenue of investigation to reduce platinum resistance in ovarian cancers.

2. Results

2.1. Characterization of CSC/MS C Heterospheroids

CSC/MS C heterospheroids (either human ovarian carcinoma OVCAR3/MS C or matched patient CSC/CA-MS C) were generated and observed to form compact, intact spheroids in hanging drop cultures by 4 days (Figure 1A). At Day 5, heterospheroids were harvested to characterize the presence of MS C within them using CD73. Flow analysis protocols were adapted from our previous studies [19–21,55,56], and gating strategy for each antibody and its associated FMO isotype are demonstrated in Figures S1–S4. Representative flow analysis plots (Figure 1B) indicate the presence of a CD73+ population within heterospheroids. Further quantification indicated the robust presence of a 5–20% CD73+ MS C population within heterospheroids at Day 5 (Figure 1C). As seen in Figure S1, CSC did not express CD73.

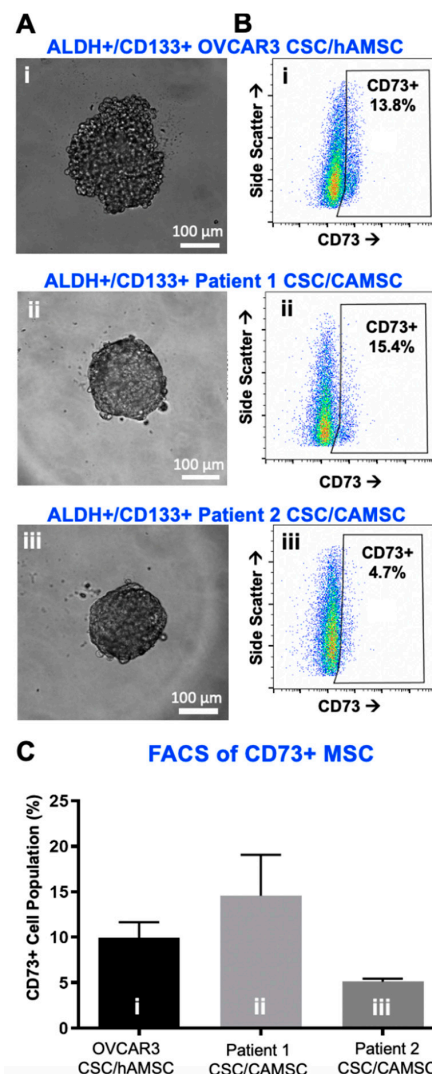


Figure 1. Characterization of ALDH+/CD133+ cancer stem-like cells (CSC)/carcinoma associated mesenchymal stem cell (CA-MS C) heterospheroids with fluorescence activated cell sorting (FACS). (A) Phase contrast micrographs of (i) OVCAR3 CSC/MS C, (ii) Patient 1 CSC/CA-MS C and (iii) Patient 2 CSC/CA-MS C heterospheroids showing compact spheroids following 4 days in hanging drop culture. (B) Representative flow cytometry plots quantifying the presence of CD73+ MS C within heterospheroids (i) OVCAR3 CSC/MS C, (ii) Patient 1 CSC/CA-MS C and (iii) Patient 2 CSC/CA-MS C heterospheroids at Day 5. See Supplementary Figures S1–S4 for gating strategies. (C) Graphical representation of flow cytometry analysis data, quantifying the presence of CD73+ MS C within heterospheroids, ranging from ~5% to 27% ($n \geq 3$).

2.2. CSC/MSC Heterospheroids Demonstrate a Platinum-Resistant Phenotype, Enriched with ALDH+ Cells

To assess the impact of MSC on cancer cell stemness, we evaluated aldehyde dehydrogenase (ALDH) activity within heterospheroids as a marker of CSC, consistent with our prior work [28]. Previous work has established ovarian cancer cells that express CD133 highly and have elevated ALDH activity, as the ALDH+ CD133+ CSC, which are at the apex of the CSC hierarchy [8,9,11,18–21,55,59]. These CSC can self-renew and asymmetrically divide to create daughter progenies that are either ALDH+ or CD133+. Therefore, ALDH+ population contains both CD133+ and CD133– cancer cells. We found significant increase in ALDH+ cells in CSC/MSC heterospheroids when compared to CSC mono-spheroids (Figure 2A,B). Significant enhancement in ALDH+ cells (* $p < 0.05$, ** $p < 0.001$, two-way ANOVA) was observed between OVCAR3 CSC and OVCAR3 CSC/MSC spheroids, as well as Patient 1 and Patient 2 CSC/CA-MSC spheroids. On average, the ALDH+ cells increased by ~1.5-fold in CSC/MSC spheroids compared to CSC spheroids alone (Figure 2B). As seen in Figure S2C, MSC did not express ALDH.

Given the elevation in ALDH activity suggestive of increased stemness, we tested the impact of MSC on carboplatin sensitivity in CSC/MSC heterospheroids. We observed a significant elevation in carboplatin IC₅₀ in CSC/MSC spheroids compared to CSC spheroids alone, in the spheroids based on OVCAR3 and primary patient samples. Representative images of control and drug treated spheroids at 100 μ M carboplatin indicate the loss of boundary integrity and toxicity induced by drug treatment (Figure 2C). Carboplatin IC₅₀ plot for each sample (Figure 2D) demonstrates significant changes in CSC/MSC spheroids. Similar to our previous observation [22], heterospheroids that contained MSC or CA-MSC were significantly more chemoresistant to carboplatin treatment, with higher IC₅₀ values compared to CSC-only spheroids (Figure 2E). Given the heterogeneity in the patient samples, the IC₅₀ values differed significantly between the heterospheroids generated with the OVCAR3 CSC and patient-derived CSC. These results are expected based on the previous characterization of patient-derived heterogeneity in the hanging drop spheroids [18–21,55].

2.3. Knockdown of MSC-Derived PDGFB Reveals the Critical Significance of PDGF-BB/PDGFR- β Signaling in Platinum Resistance and CSC Enrichment

We hypothesized that PDGF-BB/PDGFR- β signaling may be a critical pathway involved in CSC/MSC interactions. To determine the impact of MSC PDGF signaling on platinum resistance, we proceeded to knock down *PDGFB* in MSC using siRNA. Gene expression analysis indicated that siPDGFB MSC had a 74% knockdown of *PDGFB* at 96 h, compared to no knockdown in scrambled siRNA (SCR) control MSC (** $p < 0.001$, one-way ANOVA) (Figure 3A), without significant change to viability. Heterospheroids were generated from CSC/siPDGFB MSC to understand changes in platinum resistance and percentage of ALDH+ cells upon knock-down of MSC-derived PDGF-BB. PDGFR- β gene expression was significantly reduced in CSC in CSC/siPDGFB MSC heterospheroids (** $p < 0.001$, one-way ANOVA) (Figure 3B). Increase in percent ALDH+ cells observed in SCR MSC heterospheroids was significantly reduced in CSC/siPDGFB MSC spheroids (* $p < 0.05$, one-way ANOVA; Figure 3C). Along with the significantly reduced percentage of ALDH+ cells, we also observed an increased sensitivity to carboplatin treatment, evidenced by the decreased IC₅₀ values in CSC/siPDGFB MSC heterospheroids (46.2 μ M compared to 66.3 μ M in CSC/SCR MSC; Figure 3D). Heterospheroids generated from modified MSC were phenotypically very similar to unmodified MSC on phase contrast images (Figure 3E).

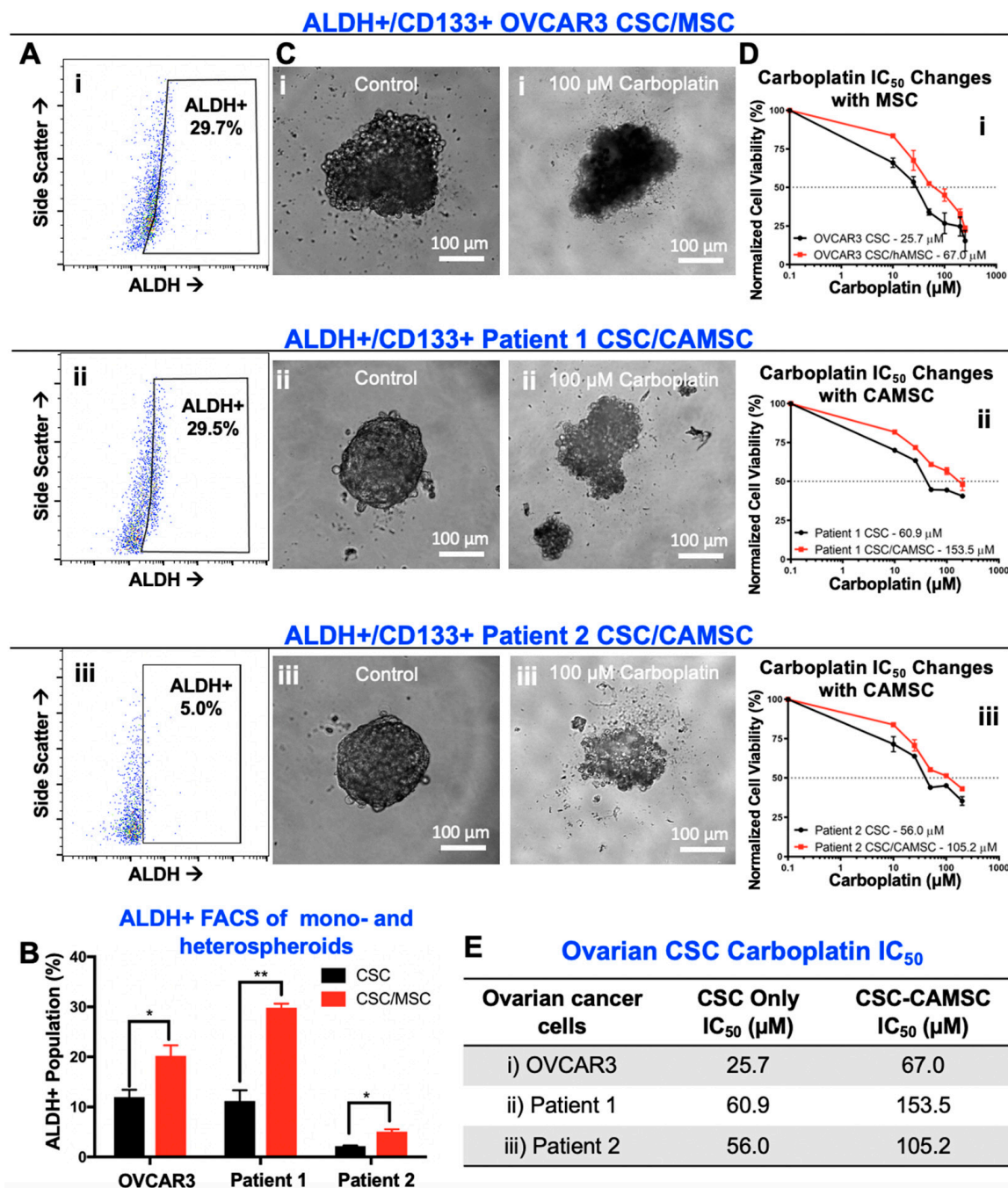


Figure 2. Co-culture of ovarian CSC with MSC leads to increased stemness and platinum resistance. (A) Representative flow cytometry plots of ALDH+ cells in (i) OVCAR3 CSC/MSC, (ii) Patient 1 CSC/CA-MSC and (iii) Patient 2 CSC/CA-MSC heterospheroids. (B) Graphical representation of ALDH+ flow cytometry analysis between CSC monospheroids, and CSC/MSC heterospheroids indicate a significant increase in ALDH+ populations in heterospheroids (* $p < 0.05$, ** $p < 0.001$, two-way ANOVA, $n \geq 3$). (C) Phase contrast micrographs of (i) OVCAR3 CSC/MSC, (ii) Patient 1 CSC/CA-MSC and (iii) Patient 2 CSC/CA-MSC Day 5 heterospheroids treated with 100 μM of carboplatin or control untreated for 48 h. Images indicate a loss of boundary integrity and cell death within carboplatin treated spheroids, compared to untreated spheroids at the same time-point. (D) Graphical representation of IC₅₀ plots derived from cell viability quantification, demonstrating that CSC/MSC heterospheroids demonstrate an increased IC₅₀ to carboplatin compared to CSC monospheroids ($n \geq 3$). (E) Tabulation of changes in IC₅₀ values with MSC/CA-MSC co-culture.

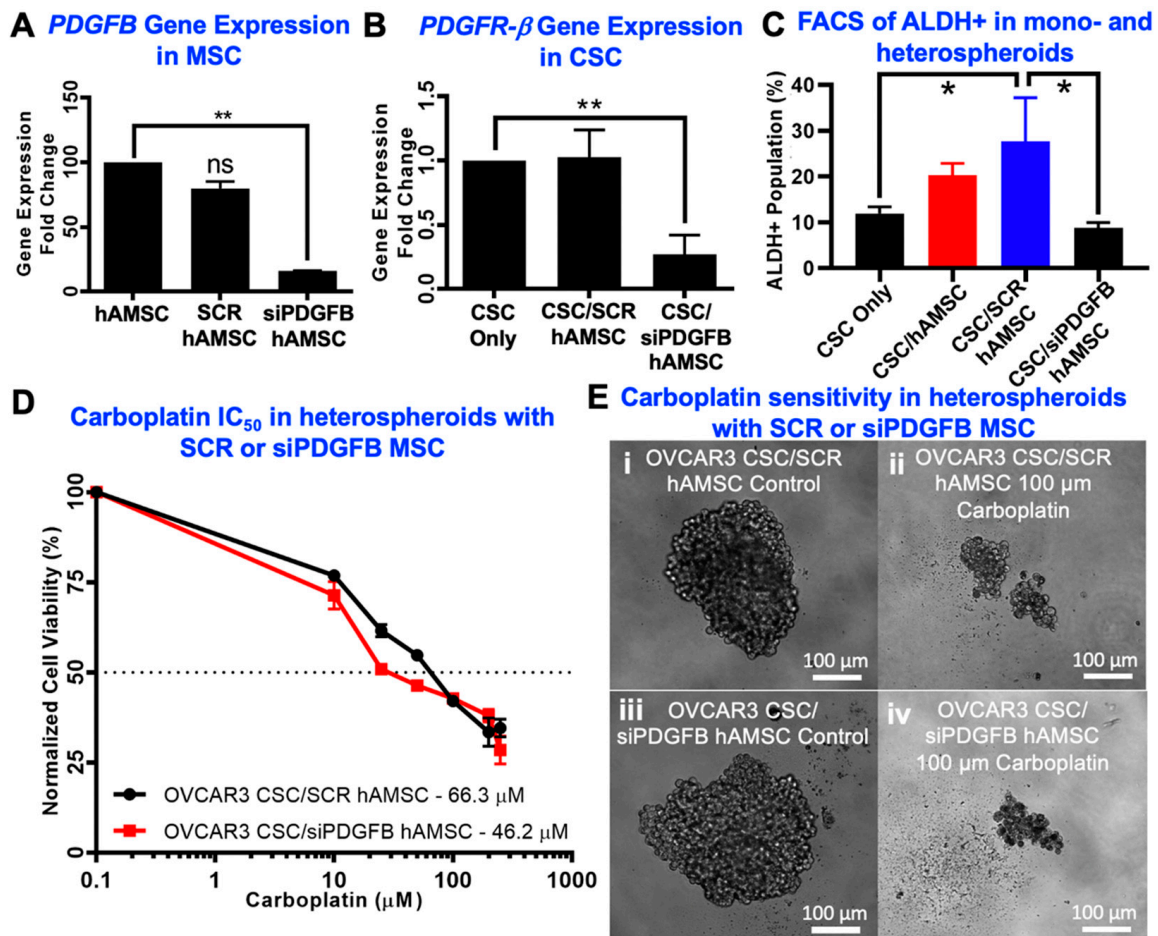


Figure 3. CSC platinum resistance and CSC enrichment can be reduced with *PDGFB* knockdown in MSC. (A) Fold change in *PDGFB* gene expression in MSCs treated with scrambled siRNA (SCR) or *PDGFB* siRNA (siPDGFB) was quantified with qPCR showing a significant decrease with siPDGFB (** $p < 0.001$, one-way ANOVA, $n \geq 3$). (B) Gene expression of the receptor, *PDGFRB* in OVCAR3 CSCs was decreased significantly when co-cultured with siPDGFB MSCs compared to CSC mono-cultures (** $p < 0.001$, one-way ANOVA, $n \geq 3$). (C) Flow cytometry of ALDH expression in OVCAR3 CSCs showed a decrease in ALDH+ cells when co-cultured with siPDGFB MSCs (* $p < 0.05$, one-way ANOVA followed by Tukey's test, $n \geq 3$). (D) Quantification of the IC₅₀ changes using an MTS assay of OVCAR3 CSCs cultured with SCR or siPDGFB MSCs showing a reduction in IC₅₀ ($n \geq 3$). (E) Representative optical microscopy images of (i) OVCAR3 CSC/SCR MSC without drug treatment, (ii) OVCAR3 CSC/SCR MSC treated with 100 μM carboplatin, (iii) OVCAR3 CSC/siPDGFB MSC without drug treatment and (iv) OVCAR3 CSC/siPDGFB MSC treated with 100 μM carboplatin.

2.4. PDGF-BB/PDGFR-β Signaling Is Significantly Involved in CSC/MSC Interactions Leading to the Development of Platinum Resistance

Given that we found PDGF-BB/PDGFR-β signaling to be a critical pathway involved in CSC/MSC interactions, we next tested interactions between soluble ligand and its receptor. In order to test the presence of PDGF-BB as a soluble factor within the CSC/MSC microenvironment, we performed an enzyme-linked immunosorbent assay (ELISA), where we found that OVCAR3 CSC cultures in CSC/MSC heterospheroids demonstrated an increased presence of PDGF-BB that was not statistically significant (Figure 4A). In order to test for PDGFR-β receptor expression in CSC, we extracted RNA from OVCAR3 CSC cultured as mono-spheroids or within CSC/MSC heterospheroids. CSC from heterospheroids were sorted by flow cytometry (for ALDH activity) before RNA isolation, to avoid

obtaining a signature from MSC. Our data indicate that upon MSC co-culture, CSCs significantly ($*** p < 0.0001$, unpaired t -test; Figure 4B) upregulate PDGFR- β expression (over two-fold).

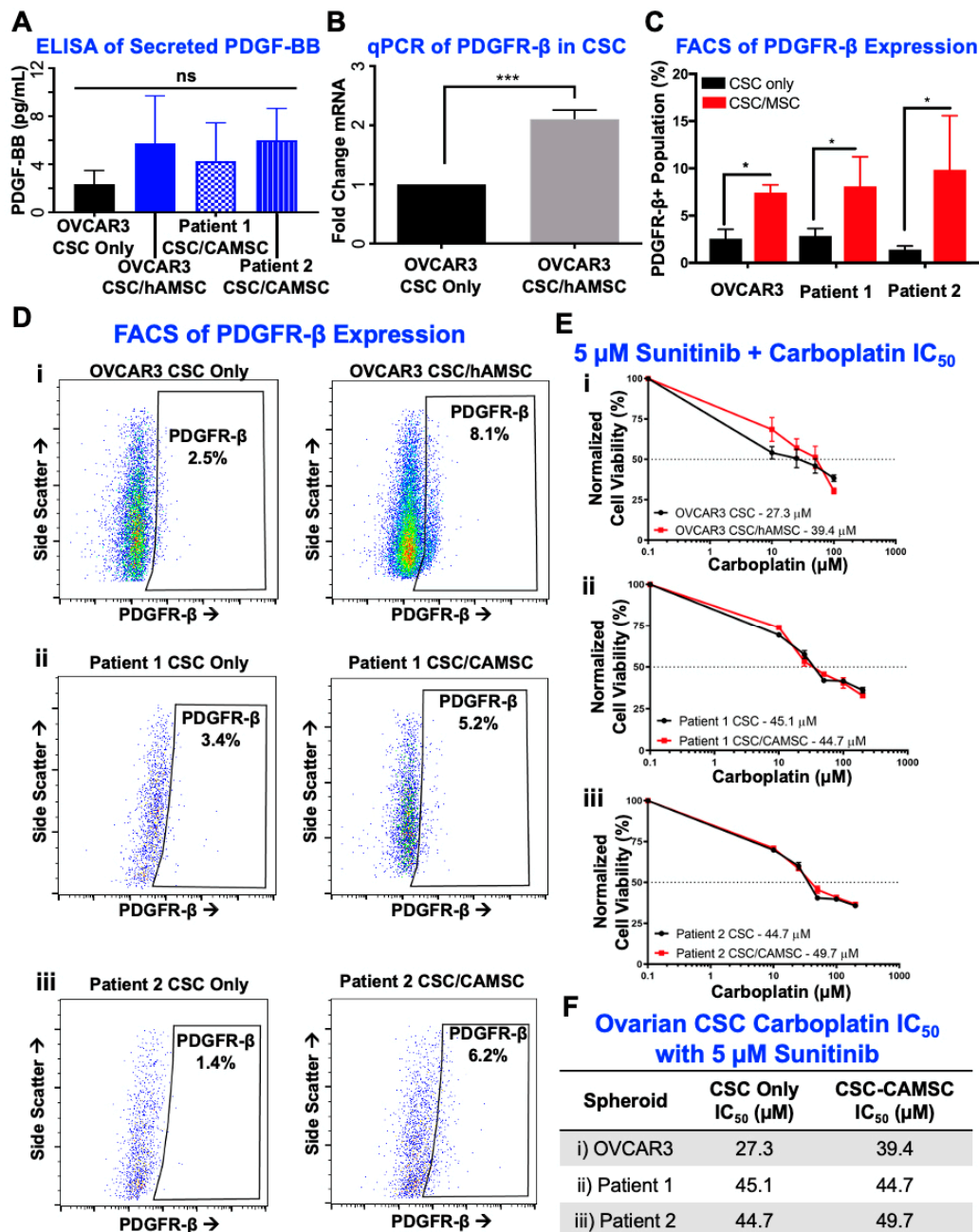


Figure 4. Involvement of PDGF-BB/PDGFR- β in CSC/MSc interactions leads to platinum resistance and can be inhibited with sunitinib. (A) Increased amounts of PDGF-BB were detected via ELISA in CSC/MSc heterospheroids, compared to CSC mono-spheroids ($n \geq 3$). (B) Gene expression analysis of the receptor *PDGFRB* demonstrated a significant ($*** p < 0.0001$, t -test, $n \geq 3$) >two-fold upregulation in OVCAR3 CSC co-cultured with MSCs compared to OVCAR3 CSC mono-cultures. (C) PDGFR- β expression was confirmed using flow cytometry, and in corroboration with qPCR data, demonstrated a non-significant increase in PDGFR- β expression in CSC/MSc heterospheroids ($* p < 0.05$, one-way ANOVA followed by Tukey’s test, $n \geq 3$). (D) Representative flow cytometry plots from the quantification in (C). (E) CSC were treated with various doses of carboplatin and 5 μ M of sunitinib, a PDGFR- β inhibitor, to determine the change in IC₅₀ with MSC co-culture. (F) Tabulation of the IC₅₀ values, indicating that sunitinib treatment significantly lowers carboplatin IC₅₀ in CSC/CA-MSc heterospheroids.

We also analyzed PDGFR- β receptor expression using flow cytometry, and observed that CSC/MSC heterospheroids had a significantly elevated expression of PDGFR- β , compared to CSC mono-spheroids (* $p < 0.05$, one-way ANOVA with Tukey's test; Figure 4C). Representative flow analysis plots for PDGFR- β expression are shown (Figure 4D). To inhibit the increased PDGF-BB/PDGFR- β signaling within CSC/MSC heterospheroids, we used sunitinib, which blocks PDGFR- β among other tyrosine kinases. Low dose sunitinib partially reversed MSC driven increases in chemotherapy resistance with a sub-cytotoxic dose of 5 μM , with IC_{50} 39–50 μM (Figure 4E,F) in the presence of sunitinib, compared to 67–153 μM without sunitinib (Figure 2D,E). Table S1 lists the carboplatin IC_{50} across all comparison groups, with and without sunitinib.

2.5. EMT Phenotype Observed Downstream of PDGF-BB/PDGFR- β Interactions in CSC

Increases in EMT transcription markers such as TWIST, SNAIL, ZEB1 and ZEB2 have been linked to increased migration and metastasis, and has previously been linked to PDGF [60,61]. We observed a significant upregulation (>two-fold) of several transcription factors associated with the EMT phenotype in OVCAR3 CSC cultured within CSC/MSC heterospheroids (Figure 5A). The same genes were significantly downregulated in CSC/siPDGFB MSC conditions (** $p < 0.0001$, two-way ANOVA) (Figure 5B), indicating the partial loss of the EMT phenotype upon loss of PDGF-BB/PDGFR- β signaling. Concurrent with upregulation of EMT genes, we observed that CSC/MSC and CSC/SCR MSC heterospheroids were significantly (* $p < 0.05$, one-way ANOVA) more migratory in a transwell setting, and this migration could be inhibited using the PDGFR- β inhibitor sunitinib or by inhibiting the secretion of PDGF-BB from MSC using siPDGFB MSC within heterospheroids (Figure 5C). Representative fluorescent micrographs are demonstrated in Figure 5D corresponding to the various conditions tested for migration.

2.6. Hedgehog Is Activated Downstream of MSC-Derived PDGFB in CSC

We previously showed that MSC induce Hedgehog signaling in CSC [22]. To determine if the PDGF-BB/PDGFR- β signaling was responsible for this alteration in Hedgehog pathway, we used qPCR to observe changes in expression of the genes associated with the Hedgehog signaling pathway (Figure 6A). We found that Hedgehog ligands SHH and IHH were significantly upregulated in CSC cultured in heterospheroids with WT MSC, and this upregulation was diminished in CSC cultured with siPDGFB MSCs (Figure 6A; **** $p < 0.0001$, two-way ANOVA). Similar patterns of gene expression were observed for downstream targets of classical Hedgehog signaling, PTCH1, SMO (* $p < 0.05$, two-way ANOVA) and GLI1 (* $p < 0.05$, two-way ANOVA), indicating the partial involvement of PDGF-BB signaling upstream of Hedgehog ligand secretion in CSC within the CSC/MSC interaction paradigm. We additionally tested if this cross-talk between PDGF-BB/PDGFR- β and Hedgehog signaling was synergistic by using a SMO inhibitor, sonidegib, at sub-cytotoxic IC_{50} doses of 1 mM. Changes in Carboplatin IC_{50} are plotted in the presence of sonidegib in Figure 6B, implying a significant cross-talk between the two tested pathways. Representative phase contrast images of spheroids treated with carboplatin in the presence of sonidegib are shown in Figure 6C. Table S1 lists the carboplatin IC_{50} across all comparison groups, with and without sonidegib.

2.7. Serial Passaging of CSC/MSC Spheroids Indicate CSC Enrichment

We have recently demonstrated that serially passaging ovarian cancer spheroids over 20 passages increases their stemness, tumorigenicity and chemoresistance [21]. In order to observe any changes in CSC enrichment modulated by co-culturing with MSC in heterospheroids, we serially passaged CSC/MSC spheroids for three consecutive passages (Passage 0–2). Three-dimensional serial passaging did not diminish the ability of CSC and MSC to form spheroids, as demonstrated by phase contrast images of spheroids at Day 1 and Day 4 (Figure 7A). Flow analysis at each passage indicated the statistically significant increase in ALDH+ cells within heterospheroids with serial passaging (** $p < 0.001$, two-way ANOVA), similar to our previous serial passage work [47], and a significant increase in PDGFR- β expression (* $p < 0.05$, two-way ANOVA). No changes in CD73 expression were noted, implying the steady maintenance of ~20% of the

heterospheroid population as MSC (Figure 7B). Furthermore, no significant changes in proliferation were observed in heterospheroids with serial passaging (Figure 7C).

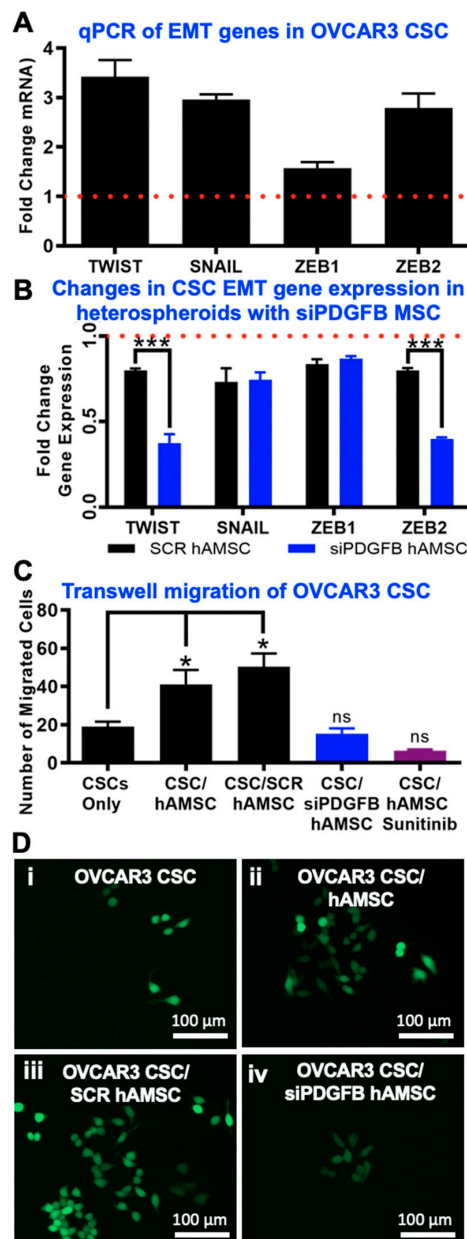


Figure 5. Downstream EMT Markers and Changes in Migration of Ovarian CSC. (A) Gene expression analysis of EMT markers in OVCAR3 CSCs cultured with MSCs in heterospheroids, compared to CSC mono-cultures (red dotted line). A significant (>two-fold) increase in gene-expression was observed for several EMT markers tested ($n \geq 3$). (B) Gene expression analysis of EMT markers following CSC/siPDGFB MSC co-cultures demonstrated a significant downregulation (** $p < 0.0001$, two-way ANOVA, $n \geq 3$) of EMT markers upon *PDGFB* knockdown. The red line indicates CSC values. (C) Increased migration of OVCAR3 CSC was seen in a transwell assay when co-cultured with MSC; this increase was negated with sunitinib treatment or *PDGFB* knockdown of MSCs ($* p < 0.05$, one-way ANOVA, $n \geq 3$). (D) Representative fluorescent images of migrated GFP+ CSC (green) in a transwell assay after 5 days of co-culture showing (i) OVCAR3 CSCs cultured alone, (ii) OVCAR3 CSC/MS, (iii) OVCAR3 CSC/SCR MSC and (iv) OVCAR3 CSC/siPDGFB MSC where more migrated cells are seen with MSC culture and siPDGFB reduces the effect MSCs have on CSC migration ($n \geq 3$). Scale bar = 100 μ m.

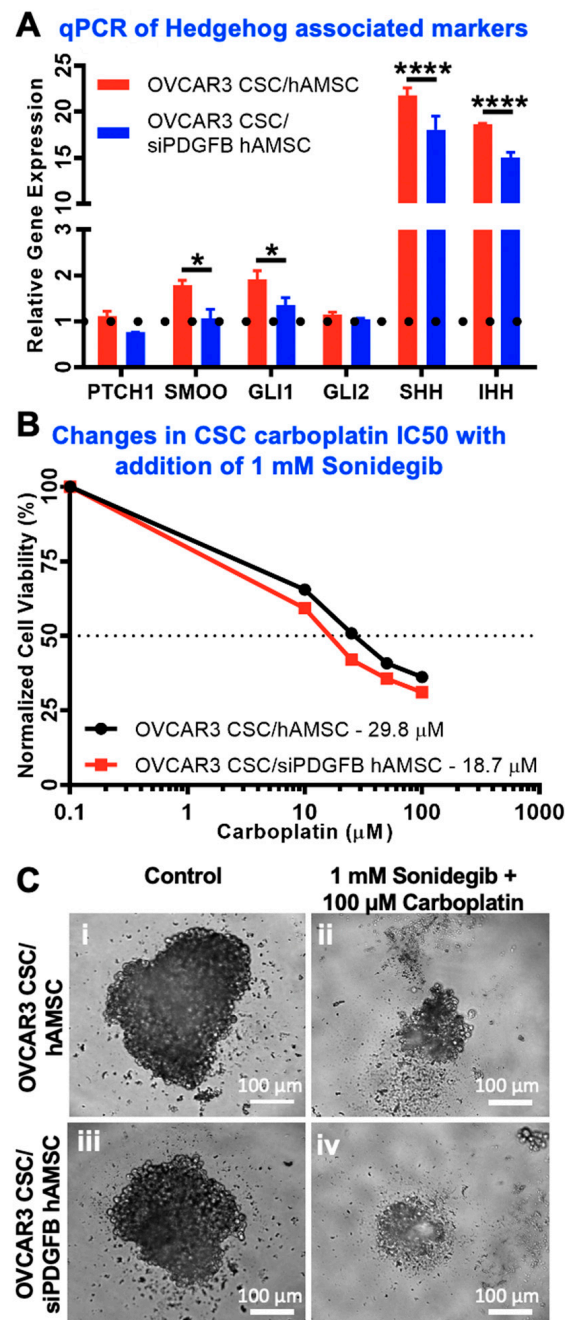


Figure 6. Downstream Activation of Hedgehog through PDGF-BB/PDGFR- β Signaling in Ovarian CSC and MSC Crosstalk. (A) Gene expression analysis of Hedgehog pathway elements in OVCAR3 CSC mono-cultures (black line), OVCAR3 CSC/MSC or OVCAR3 CSC/siPDGFB MSC heterospheroids. Gene qPCR data demonstrates a significant loss in Hedgehog ligands (*SHH* and *IHH*; **** $p < 0.0001$, two-way ANOVA, $n \geq 3$) upon PDGFB knockdown. Additionally, signaling elements within the Hedgehog pathway are also significantly downregulated (* $p < 0.05$, two-way ANOVA) upon PDGFB knockdown including Smoothed (SMOO) and *GLI1*, indicating that PDGFB might be upstream of Hedgehog ligand secretion and/or signaling ($n \geq 3$). (B) OVCAR3 CSC/MSC and OVCAR3 CSC/siPDGFB MSC heterospheroids were treated with 1 mM sonidegib, a Smoothed inhibitor, and carboplatin to determine the change in IC₅₀. Hedgehog inhibition compounded with knockdown of PDGFB, resulting in a lower carboplatin IC₅₀ in CSC/MSC heterospheroids ($n \geq 3$). (C) Representative phase contrast microscopy images of the heterospheroids when treated with 1 mM sonidegib and 100 μ M carboplatin, indicating significant visual cell death and loss of spheroid integrity.

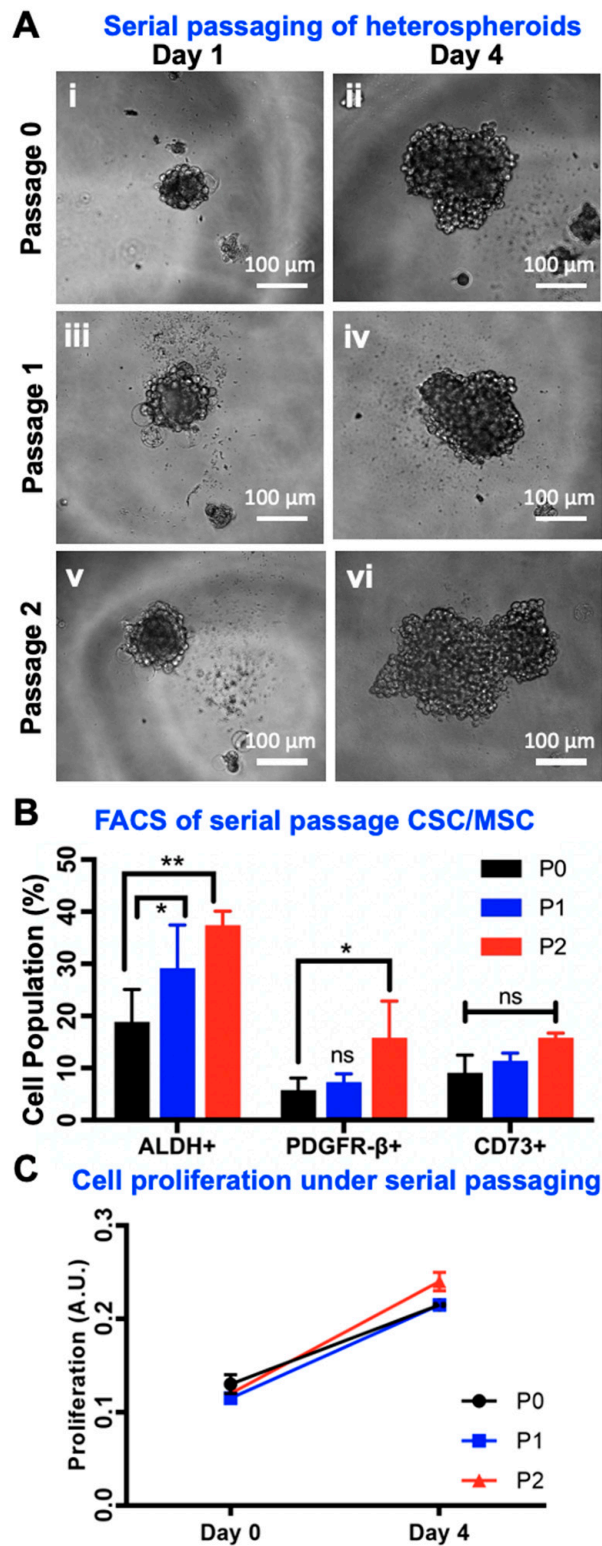


Figure 7. MSC Support the Enrichment of CSC due to Serial Passaging. (A) Representative optical microscopy images of CSC/MSCH heterospheroids on Day 1 and Day 4, Passage 0–2. (B) Quantification of the change in ALDH+, PDGFR-β and CD73+ cell populations with FACS in each passage. An increase over passage number is seen in ALDH and PDGFR-β but the CD73 population remains constant (* $p < 0.05$, ** $p < 0.001$, two-way ANOVA, $n \geq 3$). (C) Proliferation quantified on Day 0 and Day 4 was consistent across three passages (paired t -test, $n \geq 3$).

3. Discussion

Ovarian CSC are implicated in platinum resistance, disease recurrence and metastasis, leading to increased tumorigenicity and disease relapse. CSC harness the power of the tumor microenvironment (TME), including carcinoma associated mesenchymal stem cells (CA-MSC), among other stromal cells, to achieve their tumorigenic goals. The presence of CA-MSC contribute specifically to platinum resistance via multiple documented signaling pathways and mechanisms [22,29,62]. Well-established cytokine/chemokine networks exist to indicate how CA-MSC communicate with CSC and promote tumorigenesis and metastasis [11–13].

Here, we explored a novel link between the two cell types in the ovarian cancer TME, previously unknown in its involvement in CSC/CA-MSC communication, namely the PDGF-BB/PDGFR- β signaling pathway. De-regulation of PDGF-BB/PDGFR- β signaling is implicated in driving tumorigenesis and metastasis in several cancers [63–65]. PDGF-BB, the principal ligand for the PDGFR- β receptor, is significantly elevated in malignant ascites compared to non-malignant peritoneal fluid. In fact, targeting the PDGF receptors has been shown to inhibit PDGF-induced receptor activation and cell proliferation in ovarian cancer cells [66].

We found PDGFR- β receptor expression is upregulated in CSC co-cultured with MSC, likely in response to paracrine stimulation from PDGF-BB secretion by MSC. In the context of platinum resistance, our results clearly demonstrate that removing PDGF-BB from the shared CSC/MSC microenvironment through gene knockdown or inhibiting PDGF-BB/PDGFR- β interactions through sunitinib significantly improves sensitivity to carboplatin. This is generally in line with evidence in colorectal and other carcinomas where CA-MSC increase platinum resistance through a variety of mechanisms [22,29,62]. Our work demonstrates the specific involvement of the growth factor PDGF-BB in this platinum resistance phenomenon, in line with other described roles of PDGF signaling in ovarian and other cancers in their interaction with mesenchymal stroma [36,37,67]. Furthermore, in line with established literature, we observe an increase in the percentage of ALDH⁺ CSC in the heterospheroids, with an associated increase in EMT signatures, and functional migration [40,41,43,44,46,47,66]. PDGF signaling has been related to increased EMT markers such as *TWIST*, *SNAIL*, *ZEB1* and *ZEB2* through several pathways in cancer cell-MSC interactions [44,47,68,69].

The Hedgehog signaling pathway has been well-documented to promote platinum resistance and tumorigenesis of epithelial ovarian tumors, even posing as an attractive therapeutic target [70,71]. Our results indicate that CSC/MSC interactions increase the secretion of Hedgehog ligands, consistent with the bi-directional communication paradigm resulting in increased percentage of ALDH⁺ CSC via MSC-secreted BMP-4 [9]. Our studies further reveal the putative upstream involvement of PDGF-BB/PDGFR- β potentiating CSC/MSC Hedgehog signaling through *PTCH*, *SMO* and *GLI1*, all documented to result in platinum resistance of ovarian cancer [6,22,45,72]. Knockdown of MSC-derived PDGF-BB results in a significant loss of Hedgehog ligands (SHH, IHH) and pathway elements (*PTCH*, *SMO*, *GLI1*) in the CSC compartment, wholly implicating PDGF-BB to be a potent upstream regulator of Hedgehog signaling. Paracrine PDGF-BB is implicated upstream of Hedgehog, resulting in migration and cytoprotection in non-cancerous muscle cells, and several cancers including gliomas and cholangiocarcinomas [45,73–75]. Through our results, we therefore propose a novel cross-talk between PDGF-BB/PDGFR- β interactions and Hedgehog signaling in ovarian cancer, which can lead to the development of a tumorigenic, metastatic and platinum resistant phenotype within CSC, driven partially by MSC-secreted PDGF-BB (Figure 8).

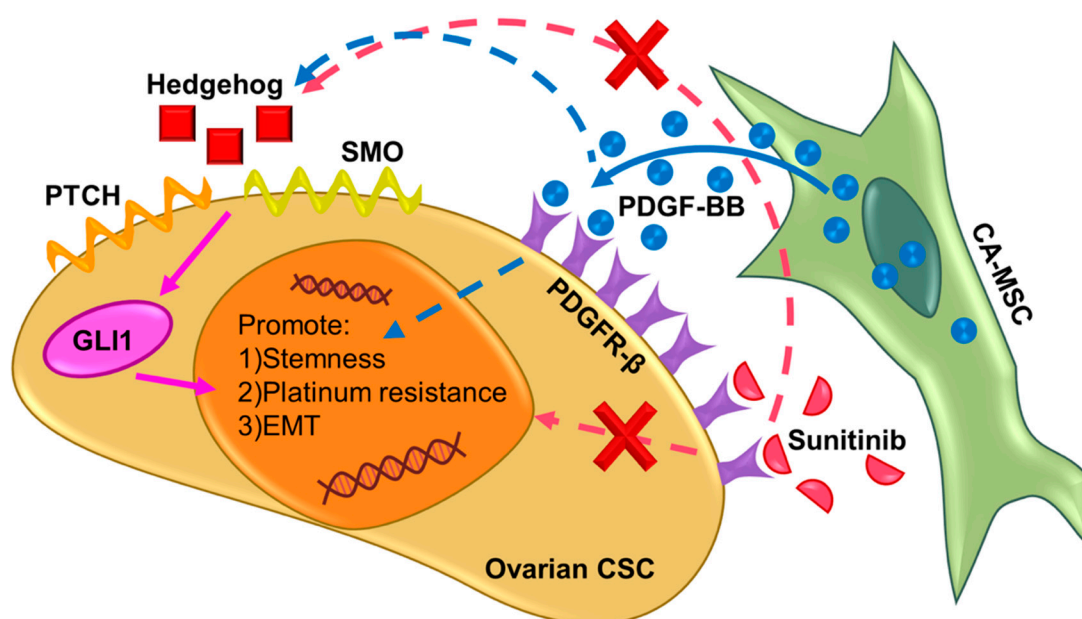


Figure 8. Hypothesized mechanism of PDGF-BB/PDGFR- β communication between ovarian CSC and CA-MSC with Hedgehog downstream signaling. PDGF-BB is secreted by CA-MSC and binds to PDGFR- β receptor, which are expressed by ovarian CSC. Binding between PDGFR- β and PDGF-BB directly causes an increase in CSC markers, platinum resistance and EMT markers in ovarian CSC. Additionally, PDGF-BB binding is shown to be upstream of Hedgehog as it leads to an increase in Hedgehog ligand secretion. Hedgehog is known to also cause an increase in CSC markers, platinum resistance and EMT markers in ovarian CSC through PTCH, SMO and GLI1. Treatment with sunitinib, a PDGFR- β inhibitor, leads to decrease in the CSC and EMT marker expression, and increase in sensitivity to platinum. These phenotypes are direct result of inhibition of the PDGF-BB/PDGFR- β and Hedgehog signaling pathways.

4. Materials and Methods

4.1. Materials

All tissue culture reagents (medium components, supplements) were purchased from Thermo Fisher Scientific (Waltham, MA, USA), unless otherwise specified. The OVCAR3 cell line was purchased from American Type Culture Collection (ATCC) (Waltham, MA, USA), and used under Passage 40. Human adipose-derived mesenchymal cells were also purchased from Thermo Fisher Scientific, and used within Passage 5. RNA interference reagents were purchased from Millipore Sigma (St. Louis, MO, USA). Matched primary dissociated live cryopreserved patient samples from high grade serous ovarian carcinoma were consented to Memorial Sloan Kettering Cancer Center IRB-approved biospecimen banking protocol and analyzed under an IRB-approved biospecimen use protocol. Sonidegib was a gift from the laboratory of Dr. Charlotte Mistretta at the University of Michigan School of Dentistry (Ann Arbor, MI, USA). The study was approved by the Memorial Sloan Kettering Cancer Center Institutional Review Board (protocol 15-200, initial approval 8/21/2015, continuing review approval 7/23/2019).

4.2. Isolation of Ovarian CSCs and CA-MSCs from Ovarian Cancer Patient Samples

CSC were isolated from the OVCAR3 cell line, or two high-grade serous ovarian carcinomas (Patient 1 and Patient 2), using protocols outlined previously [19,55–58]. Briefly, single cell suspensions were incubated with ALDEFLUOR reagent (Stem Cell Technologies, Vancouver, BC, Canada), and CD133 antibody. In this work, we define the 'ALDH+ cells' as the 'viable cells that possess high ALDH activity

in the ALDEFLOUR FACS assay. ALDH⁺/CD133⁺ cells were isolated using fluorescent activated cell sorting on the Beckman Coulter MoFlo Astrios, by trained technicians.

For CA-MSc from single cell tumor suspensions, cells were plated onto two-dimensional (2D) tissue culture treated plates in an MSC selection medium following protocols outlined previously [28]. The medium consisted of basal MEBM (Lonza, Walkersville, MD, USA), supplemented with 20 ng/mL EGF, bFGF, 1× B27, 5 µg/mL Insulin, 100 µM β-mercaptoethanol, 1 ng/mL hydrocortisone, 1× antibiotics/antimycotics and 10% fetal bovine serum. Adherent cells were CA-MSc.

4.3. RNA Interference of PDGFB in MSC

Validated siRNA duplex constructs targeted against human PDGFB were purchased from Sigma Aldrich (SASI_Hs01_00121961, SASI_Hs01_00121962, (St. Louis, MO, USA). Mission siRNA Transfection reagent (Sigma Aldrich) was used to reverse transfect 10 nM of siRNA to MSC, in a 24-well format following manufacturer's protocols. A universal negative siRNA non-targeting control (Sigma Aldrich) was utilized to rule out effects from transfection protocols. RNA was extracted from MSC treated with siRNA (siPDGFB MSC) to assess the amount of knockdown via qPCR, outlined below.

4.4. Formation of Mono- and Heterospheroids from CSC and MSC

Mono- or heterospheroids were generated on an in vitro 384 well hanging drop array platform as described previously [19,55–58]. Briefly, to generate CSC monospheroids, single cell suspensions of CSC were diluted, in such a manner that a 20 µL drop contained 12 CSCs. For heterospheroids, CSC and MSC were diluted in a 1:3 ratio, such that a 20 µL drop contained three CSCs and nine MSCs. Spheroids were cultured in a 1:1 medium mixture of RPMI and ADSC-BM (Lonza) supplemented with 1% penicillin/streptomycin and 1% L-glutamate. Live cell imaging using phase contrast microscopy was utilized to follow the formation of CSC or CSC/MSc spheroids. Spheroids were generated from CSCs isolated from the OVCAR3 cell line, or OVCAR3 CSCs with human adipose MSC (MSC). Two matched patient samples (Patient 1 and Patient 2) were also utilized to generate CSC/CA-MSc spheroids.

Additionally, heterospheroids were manufactured from CSC and siPDGFB MSC, in order to assess changes in platinum resistance and CSC characteristics within heterospheroids. CSC^{gfp}/siPDGFB MSC heterospheroids were also generated, to be able to isolate the CSC^{gfp} compartment using fluorescent activated cell sorting using protocols described previously [20], for subsequent qPCR analysis.

4.5. Flow Cytometry Analysis

At the end of 4 days in spheroid culture, mono- or heterospheroids were harvested and resuspended in FACS Buffer (PBS + 2% fetal bovine serum). The presence of MSC was determined by staining with CD73. CSC were identified using elevated ALDH activity using the ALDEFLOUR Kit. The presence of PDGFR-β (CD340) was assessed by staining with PDGFR-β antibody. Flow analysis protocols were adapted from our previous studies [19–21,55,56], and gating strategies are demonstrated in Supplementary Information Figures S1–S4.

4.6. Quantification of Cytokines Using ELISA

For ELISA assays, medium was harvested from 100 spheroids (CSC, CSC/CA-MSc spheroids). ELISA assays were performed using the Duoset ELISA system (R&D Biosystems, Minneapolis MN) following the manufacturer's protocol, modified to include an overnight incubation. PDGF-BB was analyzed using a standard curve, and a four parametric ELISA curve generation. ELISA assays and data analysis were performed at the Immunological Monitoring Core at the Rogel Cancer Center, University of Michigan (Ann Arbor, MI, USA).

4.7. Assessment of Chemoresistance in Spheroids

Spheroids were generated from CSC, CSC/MSC or CSC/siPDGFB MSC and allowed to form until Day 5. To identify changes in IC₅₀ for carboplatin, spheroids were treated with a range of concentrations of Carboplatin (10–200 µM) for 48 h. The MTS viability assay (Abcam, Cambridge, UK) was used to determine viability of control untreated and carboplatin-treated spheroids, following manufacturer's protocols. Following a 1.5-h incubation of the MTS reagent with spheroids at 37 °C, absorbance was read at 590 nm following manufacturer's protocols. Results were quantified as normalized cell viability, based on the viability of untreated control spheroids. Experiments were repeated with three–five biological replicates for statistical analysis, and each experiment contained >20 technical replicates. For combination drug doses, a range of carboplatin was utilized along with Sunitinib 5 µM, or Sonidegib 1 mM, to identify changes in IC₅₀.

4.8. Assessment of Migration in Spheroids

In order to quantify invasiveness of heterospheroids, 8 µm transwell inserts were placed in each well of a 24-well plate. Ten CSC^{gfp} or CSC^{gfp}/MSC spheroids were harvested at Day 5 from hanging drop arrays, and a single cell suspension was made. The cells were then FACS-sorted for the GFP expression [20]. GFP-positive single cells were placed on the top chamber of a transwell insert. The bottom chamber was filled with 400 µL of fresh medium, thus, only the bottom of the transwell insert was immersed in medium. Following 3 days, the transwell insert was removed, and several images of the bottom of the 24-well plate were obtained using fluorescent microscopy, identifying GFP+ cells. Image J (U.S. National Institutes of Health, Bethesda, MD, USA) was used to quantify the number of cells in a field of view. At least four random non-overlapping fields of view were counted from each experiment, to find the number of cells that migrated through the transwell insert to the bottom of the well.

4.9. Gene Expression Analysis via qPCR

RNA was extracted from spheroids or cells using the RNeasy extraction kit (Qiagen, Hilden, Germany). Extracted RNA was assessed for concentration and purity using a Nanodrop 2000 (Thermo Fisher Scientific) spectrophotometer. RNA was transcribed to cDNA using the High-fidelity cDNA Transcription kit (Life Technologies, Carlsbad, CA, USA), and qPCR was carried out in a 96-well format using 7900HT (Applied Biosystems, Foster City, CA, USA). Gene expression differences were quantified using the $2\Delta\Delta C_T$ method, using GAPDH as the housekeeping control, and reported as fold change compared to a control sample. The following primers were utilized to test changes in EMT: *TWIST*, *SNAIL*, *ZEB1*, *ZEB2*; the following primers were utilized to test PDGF signaling: *PDGFB*, *PDGFRB*; the following primers were used to test Hedgehog signaling: *PTCH1*, *SMOO*, *GLI1*, *GLI2*, *SHH*, *IHH*. A list of all primers used in qPCR is provided in Table S2.

For qPCR experiments, RNA was isolated from CSC mono-spheroids, or CSCs isolated based on a GFP label from CSC^{gfp}/MSC heterospheroids or CSC^{gfp}/siPDGFB MSC spheroids. Control comparisons were made with CSC mono-spheroids using the $2\Delta\Delta C_T$ method, and fold changes are reported.

4.10. Serial Passaging of CSC/MSC Heterospheroids

In order to assess CSC enrichment, and predict tumorigenicity of CSC/MSC heterospheroids, we utilized an in vitro serial passage model [20,21]. Passage 0 (P0) spheroids were generated using protocols outlined in Section 4.4. Following 4–5 days of heterospheroid culture, spheroids were harvested and CSC were isolated based on elevated ALDH activity using fluorescent activated cell sorting. Isolated CSC were combined with MSC again and seeded into heterospheroids, and allowed to remain in non-adherent hanging drop culture for 4–5 days. This process was repeated four times, until a terminal passage of P3 was reached. At the end of each passage, spheroids were also harvested to analyze the expression of ALDH activity, and PDGFR-β and the maintenance of a CD73+

MSC population, using flow cytometry. Proliferation was assessed in spheroids by comparing MTS absorbance in Day 1 compared to Day 4.

4.11. Data Analysis and Statistics

All experiments were performed with three–five biological replicates, with at least 20 technical replicates for drug viability and at least three technical replicates for qPCR. Statistical analysis was performed using GraphPad Prism 8 for Mac Os X (www.graphpad.com). Appropriate statistical tests were performed and reported in each graph/figure legend, with asterisks indicating any significant differences in test variables.

5. Conclusions

In conclusion, we have found PDGF-BB/PDGF- β to be an important signaling pathway between CA-MSC and CSC in ovarian cancer, which has yet to be fully studied. We have linked PDGF-BB/PDGF- β with increased stemness, metastatic potential and platinum resistance in ovarian CSC, acting in part via canonical Hedgehog signaling. Inhibition of PDGF-BB/PDGF- β signaling was found to reduce platinum resistance and metastatic potential development in ovarian CSC. Our findings suggest that this PDGF-BB/PDGF- β pathway holds much interest for future studies in designing more effective therapies for ovarian cancer. Overall, our report underscores the importance of TME signaling, and suggests that in order to effectively target ovarian cancers, the tumor cells, as well as the supporting stromal cells, are important, and need to be considered together.

Supplementary Materials: The following are available online at <http://www.mdpi.com/2072-6694/12/8/2063/s1>, Figure S1: FACS gating strategy for CD73 expression in OVCAR3 and patient-derived CSC. FMO isotype for CD73 expression in (A) OVCAR3 CSC, (B) Patient 1 CSC and (C) Patient 2 CSC, Figure S2: FACS gating strategy for MSC expression of CD73, CD105 and ALDH, Figure S3: FACS gating strategy for siPDGFB-MSC CD73 expression, Figure S4: FACS gating strategy for PDGF- β and ALDH in patient CSC, Table S1: Summary of Carboplatin IC₅₀ Values in OVCAR3/MSC heterospheroids, Table S2: Primers used in qPCR.

Author Contributions: Conceptualization, G.M.; Data curation, S.R., C.S.S. and A.W.; Formal analysis, S.R. and C.S.S.; Funding acquisition, G.M.; Investigation, A.W. and G.M.; Methodology, S.R., A.W. and G.M.; Project administration, G.M.; Resources, K.M., D.Z., R.J.B. and G.M.; Supervision, G.M.; Validation, A.W.; Visualization, C.S.S.; Writing—original draft, S.R., C.S.S., A.W. and G.M.; Writing—review and editing, K.M., D.Z., R.J.B. and G.M. All authors have read and agreed to the published version of the manuscript.

Funding: This work is supported primarily by the American Cancer Society Research Scholar Award RSG-19-003-01-CCE (G.M.), DOD OCRP Early Career Investigator Award W81XWH-13-1-0134 (G.M.), DOD Pilot award W81XWH-16-1-0426 (G.M.), DOD Investigator Initiated award W81XWH-18-0346 (G.M.), Rivkin Center for Ovarian Cancer (G.M.), Michigan Ovarian Cancer Alliance (G.M.), NIH/NIDCR Tissue Engineering and Regeneration Training Grant T32DE00007057 (S.R.) and the Rackham Research Grant (C.S.S.). Research reported in this publication was supported by the National Cancer Institute of the National Institutes of Health under award number P30CA046592.

Acknowledgments: The authors acknowledge the efforts of Joel Whitfield from the Immunological Monitoring Core at the Rogel Cancer Center, for performing ELISA measurements. The authors are thankful to Mark Savary at the Flow Cytometry Core for technical assistance in performing fluorescent activated cell sorting. The authors are thankful to Elise M.-A. Fleck for conducting preliminary experiments. The authors are also grateful to Pooja Mehta and Michael Bregenzer for their contribution to this work.

Conflicts of Interest: The authors declare no conflict of interest. The funders had no role in the design of the study; in the collection, analyses or interpretation of data; in the writing of the manuscript, or in the decision to publish the results.

References

1. Ghoneum, A.; Afify, H.; Salih, Z.; Kelly, M.; Said, N. Role of tumor microenvironment in ovarian cancer pathobiology. *Oncotarget* **2018**, *9*, 22832–22849. [[CrossRef](#)] [[PubMed](#)]
2. Siegel, R.L.; Miller, K.D.; Jemal, A. Cancer statistics, 2019. *CA Cancer J. Clin.* **2019**, *69*, 7–34. [[CrossRef](#)] [[PubMed](#)]

3. Al-Alem, L.F.; Pandya, U.M.; Baker, A.T.; Bellio, C.; Zarrella, B.D.; Clark, J.; DiGloria, C.M.; Rueda, B.R. Ovarian cancer stem cells: What progress have we made? *Int. J. Biochem. Cell Biol.* **2019**, *107*, 92–103. [[CrossRef](#)]
4. Lupia, M.; Cavallaro, U. Ovarian cancer stem cells: Still an elusive entity? *Mol. Cancer* **2017**, *16*, 64. [[CrossRef](#)] [[PubMed](#)]
5. Stack, M.S.; Nephew, K.P.; Burdette, J.E.; Mitra, A.K. The Tumor Microenvironment of High Grade Serous Ovarian Cancer. *Cancers* **2018**, *11*, 21. [[CrossRef](#)]
6. Steg, A.D.; Bevis, K.S.; Katre, A.A.; Ziebarth, A.; Alvarez, R.D.; Zhang, K.; Conner, M.; Landen, C.N. Stem cell pathways contribute to clinical chemoresistance in ovarian cancer. *Clin. Cancer Res.* **2012**, *18*, 869–881. [[CrossRef](#)]
7. Zhang, B.; Chen, F.; Xu, Q.; Han, L.; Xu, J.; Gao, L.; Sun, X.; Li, Y.; Li, Y.; Qian, M.; et al. Revisiting ovarian cancer microenvironment: A friend or a foe? *Protein Cell* **2018**, *9*, 674–692. [[CrossRef](#)]
8. Silva, I.A.; Bai, S.; McLean, K.; Yang, K.; Griffith, K.; Thomas, D.; Ginestier, C.; Johnston, C.; Kueck, A.; Reynolds, R.K.; et al. Aldehyde dehydrogenase in combination with CD133 defines angiogenic ovarian cancer stem cells that portend poor patient survival. *Cancer Res.* **2011**, *71*, 3991–4001. [[CrossRef](#)]
9. Landen, C.N., Jr.; Goodman, B.; Katre, A.A.; Steg, A.D.; Nick, A.M.; Stone, R.L.; Miller, L.D.; Mejia, P.V.; Jennings, N.B.; Gershenson, D.M.; et al. Targeting aldehyde dehydrogenase cancer stem cells in ovarian cancer. *Mol. Cancer Ther.* **2010**, *9*, 3186–3199. [[CrossRef](#)]
10. Zhang, J.; Guo, X.; Chang, D.Y.; Rosen, D.G.; Mercado-Uribe, I.; Liu, J. CD133 expression associated with poor prognosis in ovarian cancer. *Mod. Pathol.* **2012**, *25*, 456–464. [[CrossRef](#)]
11. Choi, Y.J.; Ingram, P.N.; Yang, K.; Coffman, L.; Iyengar, M.; Bai, S.; Thomas, D.G.; Yoon, E.; Buckanovich, R.J. Identifying an ovarian cancer cell hierarchy regulated by bone morphogenetic protein 2. *Proc. Natl. Acad. Sci. USA* **2015**, *112*, E6882–E6888. [[CrossRef](#)] [[PubMed](#)]
12. Curley, M.D.; Therrien, V.A.; Cummings, C.L.; Sergent, P.A.; Koulouris, C.R.; Friel, A.M.; Roberts, D.J.; Seiden, M.V.; Scadden, D.T.; Rueda, B.R.; et al. CD133 expression defines a tumor initiating cell population in primary human ovarian cancer. *Stem Cells* **2009**, *27*, 2875–2883. [[CrossRef](#)] [[PubMed](#)]
13. Sharrow, A.C.; Perkins, B.; Collector, M.I.; Yu, W.; Simons, B.W.; Jones, R.J. Characterization of aldehyde dehydrogenase 1 high ovarian cancer cells: Towards targeted stem cell therapy. *Gynecol. Oncol.* **2016**, *142*, 341–348. [[CrossRef](#)] [[PubMed](#)]
14. Zhou, Q.; Chen, A.; Song, H.; Tao, J.; Yang, H.; Zuo, M. Prognostic value of cancer stem cell marker CD133 in ovarian cancer: A meta-analysis. *Int. J. Clin. Exp. Med.* **2015**, *8*, 3080–3088. [[PubMed](#)]
15. Baba, T.; Convery, P.A.; Matsumura, N.; Whitaker, R.S.; Kondoh, E.; Perry, T.; Huang, Z.; Bentley, R.C.; Mori, S.; Fujii, S.; et al. Epigenetic regulation of CD133 and tumorigenicity of CD133+ ovarian cancer cells. *Oncogene* **2009**, *28*, 209–218. [[CrossRef](#)]
16. Kryczek, I.; Liu, S.; Roh, M.; Vatan, L.; Szeliga, W.; Wei, S.; Banerjee, M.; Mao, Y.; Kotarski, J.; Wicha, M.S.; et al. Expression of aldehyde dehydrogenase and CD133 defines ovarian cancer stem cells. *Int. J. Cancer* **2012**, *130*, 29–39. [[CrossRef](#)]
17. Murphy, S.K. Targeting ovarian cancer-initiating cells. *Anticancer Agents Med. Chem.* **2010**, *10*, 157–163. [[CrossRef](#)]
18. Mehta, P.; Novak, C.; Raghavan, S.; Ward, M.; Mehta, G. Self-Renewal and CSCs In Vitro Enrichment: Growth as Floating Spheres. *Methods Mol. Biol.* **2018**, *1692*, 61–75. [[CrossRef](#)]
19. Raghavan, S.; Mehta, P.; Ward, M.R.; Bregenzler, M.E.; Fleck, E.M.A.; Tan, L.; McLean, K.; Buckanovich, R.J.; Mehta, G. Personalized Medicine-Based Approach to Model Patterns of Chemoresistance and Tumor Recurrence Using Ovarian Cancer Stem Cell Spheroids. *Clin. Cancer Res.* **2017**, *23*, 6934–6945. [[CrossRef](#)]
20. Raghavan, S.; Mehta, P.; Xie, Y.; Lei, Y.L.; Mehta, G. Ovarian cancer stem cells and macrophages reciprocally interact through the WNT pathway to promote pro-tumoral and malignant phenotypes in 3D engineered microenvironments. *J. Immunother. Cancer* **2019**, *7*, 190. [[CrossRef](#)]
21. Ward Rashidi, M.R.; Mehta, P.; Bregenzler, M.; Raghavan, S.; Fleck, E.M.; Horst, E.N.; Harissa, Z.; Ravikumar, V.; Brady, S.; Bild, A.; et al. Engineered 3D Model of Cancer Stem Cell Enrichment and Chemoresistance. *Neoplasia* **2019**, *21*, 822–836. [[CrossRef](#)]
22. Coffman, L.G.; Choi, Y.J.; McLean, K.; Allen, B.L.; Magliano, M.P.D.; Buckanovich, R.J. Human carcinoma-associated mesenchymal stem cells promote ovarian cancer chemotherapy resistance via a BMP4/HH signaling loop. *Oncotarget* **2016**, *7*, 6916–6932. [[CrossRef](#)]

23. Karnoub, A.E.; Dash, A.B.; Vo, A.P.; Sullivan, A.; Brooks, M.W.; Bell, G.W.; Richardson, A.L.; Polyak, K.; Tubo, R.; Weinberg, R.A. Mesenchymal stem cells within tumour stroma promote breast cancer metastasis. *Nature* **2007**, *449*, 557–563. [[CrossRef](#)]
24. Rynne-Vidal, A.; Au-Yeung, C.L.; Jiménez-Heffernan, J.A.; Pérez-Lozano, M.L.; Cremades-Jimeno, L.; Bárcena, C.; Cristóbal-García, I.; Fernández-Chacón, C.; Yeung, T.L.; Mok, S.C.; et al. Mesothelial-to-mesenchymal transition as a possible therapeutic target in peritoneal metastasis of ovarian cancer. *J. Pathol.* **2017**, *242*, 140–151. [[CrossRef](#)] [[PubMed](#)]
25. Spaeth, E.L.; Dembinski, J.L.; Sasser, A.K.; Watson, K.; Klopp, A.; Hall, B.; Andreeff, M.; Marini, F. Mesenchymal Stem Cell Transition to Tumor-Associated Fibroblasts Contributes to Fibrovascular Network Expansion and Tumor Progression. *PLoS ONE* **2009**, *4*. [[CrossRef](#)] [[PubMed](#)]
26. Cho, J.A.; Park, H.; Lim, E.H.; Kim, K.H.; Choi, J.S.; Lee, J.H.; Shin, J.W.; Lee, K.W. Exosomes from ovarian cancer cells induce adipose tissue-derived mesenchymal stem cells to acquire the physical and functional characteristics of tumor-supporting myofibroblasts. *Gynecol. Oncol.* **2011**, *123*, 379–386. [[CrossRef](#)] [[PubMed](#)]
27. Ding, D.C.; Liu, H.W.; Chu, T.Y. Interleukin-6 from Ovarian Mesenchymal Stem Cells Promotes Proliferation, Sphere and Colony Formation and Tumorigenesis of an Ovarian Cancer Cell Line SKOV3. *J. Cancer* **2016**, *7*, 1815–1823. [[CrossRef](#)]
28. McLean, K.; Gong, Y.; Choi, Y.; Deng, N.; Yang, K.; Bai, S.; Cabrera, L.; Keller, E.; McCauley, L.; Cho, K.R.; et al. Human ovarian carcinoma-associated mesenchymal stem cells regulate cancer stem cells and tumorigenesis via altered BMP production. *J. Clin. Investig.* **2011**, *121*, 3206–3219. [[CrossRef](#)]
29. Castells, M.; Milhas, D.; Gandy, C.; Thibault, B.; Rafii, A.; Delord, J.P.; Couderc, B. Microenvironment mesenchymal cells protect ovarian cancer cell lines from apoptosis by inhibiting XIAP inactivation. *Cell Death Dis.* **2013**, *4*, e887. [[CrossRef](#)]
30. Zhang, Y.; Dong, W.; Wang, J.; Cai, J.; Wang, Z. Human omental adipose-derived mesenchymal stem cell-conditioned medium alters the proteomic profile of epithelial ovarian cancer cell lines in vitro. *Oncotargets Ther.* **2017**, *10*, 1655–1663. [[CrossRef](#)]
31. Ng, F.; Boucher, S.; Koh, S.; Sastry, K.S.R.; Chase, L.; Lakshmipathy, U.; Choong, C.; Yang, Z.; Vemuri, M.C.; Rao, M.S.; et al. PDGF, TGF- β , and FGF signaling is important for differentiation and growth of mesenchymal stem cells (MSCs): Transcriptional profiling can identify markers and signaling pathways important in differentiation of MSCs into adipogenic, chondrogenic, and osteogenic lineages. *Blood* **2008**, *112*, 295–307. [[CrossRef](#)] [[PubMed](#)]
32. Zhang, J.M.; Feng, F.E.; Wang, Q.M.; Zhu, X.L.; Fu, H.X.; Xu, L.P.; Liu, K.Y.; Huang, X.J.; Zhang, X.H. Platelet-Derived Growth Factor-BB Protects Mesenchymal Stem Cells (MSCs) Derived From Immune Thrombocytopenia Patients Against Apoptosis and Senescence and Maintains MSC-Mediated Immunosuppression. *Stem Cells Transl. Med.* **2016**, *5*, 1631–1643. [[CrossRef](#)] [[PubMed](#)]
33. Apte, S.M.; Bucana, C.D.; Killion, J.J.; Gershenson, D.M.; Fidler, I.J. Expression of platelet-derived growth factor and activated receptor in clinical specimens of epithelial ovarian cancer and ovarian carcinoma cell lines. *Gynecol. Oncol.* **2004**, *93*, 78–86. [[CrossRef](#)] [[PubMed](#)]
34. Dabrow, M.B.; Francesco, M.R.; McBrearty, F.X.; Caradonna, S. The Effects of Platelet-Derived Growth Factor and Receptor on Normal and Neoplastic Human Ovarian Surface Epithelium. *Gynecol. Oncol.* **1998**, *71*, 29–37. [[CrossRef](#)]
35. Versnel, M.A.; Haarbrink, M.; Langerak, A.W.; Laat, P.A.J.M.d.; Hagemeyer, A.; Kwast, T.H.v.d.; Berg-Bakker, L.A.M.v.d.; Schrier, P.I. Human ovarian tumors of epithelial origin express PDGF in vitro and in vivo. *Cancer Genet. Cytogenet.* **1994**, *73*, 60–64. [[CrossRef](#)]
36. Weigel, M.T.; Rath, K.; Alkatout, I.; Wenners, A.S.; Schem, C.; Maass, N.; Jonat, W.; Mundhenke, C. Nilotinib in Combination with Carboplatin and Paclitaxel Is a Candidate for Ovarian Cancer Treatment. *Oncology* **2014**, *87*, 232–245. [[CrossRef](#)]
37. Chang, K.K.; Yoon, C.; Yi, B.C.; Tap, W.D.; Simon, M.C.; Yoon, S.S. Platelet-derived growth factor receptor- α and - β promote cancer stem cell phenotypes in sarcomas. *Oncogenesis* **2018**, *7*, 47. [[CrossRef](#)]
38. Donnem, T.; Al-Saad, S.; Al-Shibli, K.; Andersen, S.; Busund, L.T.; Bremnes, R.M. Prognostic Impact of Platelet-Derived Growth Factors in Non-small Cell Lung Cancer Tumor and Stromal Cells. *J. Thorac. Oncol.* **2008**, *3*, 963–970. [[CrossRef](#)]
39. Farooqi, A.A.; Siddik, Z.H. Platelet-derived growth factor (PDGF) signalling in cancer: Rapidly emerging signalling landscape. *Cell Biochem. Funct.* **2015**, *33*, 257–265. [[CrossRef](#)]

40. Huang, F.; Wang, M.; Yang, T.; Cai, J.; Zhang, Q.; Sun, Z.; Wu, X.; Zhang, X.; Zhu, W.; Qian, H.; et al. Gastric cancer-derived MSC-secreted PDGF-DD promotes gastric cancer progression. *J. Cancer Res. Clin. Oncol.* **2014**, *140*, 1835–1848. [[CrossRef](#)]
41. Huang, Y.; Hoffman, C.; Rajappa, P.; Kim, J.H.; Hu, W.; Huse, J.; Tang, Z.; Li, X.; Weksler, B.; Bromberg, J.; et al. Oligodendrocyte Progenitor Cells Promote Neovascularization in Glioma by Disrupting the Blood–Brain Barrier. *Cancer Res.* **2014**, *74*, 1011–1021. [[CrossRef](#)]
42. Jackson, E.L.; Garcia-Verdugo, J.M.; Gil-Perotin, S.; Roy, M.; Quinones-Hinojosa, A.; VandenBerg, S.; Alvarez-Buylla, A. PDGFR α -Positive B Cells Are Neural Stem Cells in the Adult SVZ that Form Glioma-like Growths in Response to Increased PDGF Signaling. *Neuron* **2006**, *51*, 187–199. [[CrossRef](#)] [[PubMed](#)]
43. Pinto, M.P.; Dye, W.W.; Jacobsen, B.M.; Horwitz, K.B. Malignant stroma increases luminal breast cancer cell proliferation and angiogenesis through platelet-derived growth factor signaling. *BMC Cancer* **2014**, *14*. [[CrossRef](#)]
44. Devarajan, E.; Song, Y.H.; Krishnappa, S.; Alt, E. Epithelial–mesenchymal transition in breast cancer lines is mediated through PDGF-D released by tissue-resident stem cells. *Int. J. Cancer* **2012**, *131*, 1023–1031. [[CrossRef](#)] [[PubMed](#)]
45. Fingas, C.D.; Bronk, S.F.; Werneburg, N.W.; Mott, J.L.; Guicciardi, M.E.; Cazanave, S.C.; Mertens, J.C.; Sirica, A.E.; Gores, G.J. Myofibroblast-derived PDGF-BB Promotes Hedgehog Survival Signaling in Cholangiocarcinoma Cells. *Hepatology* **2011**, *54*, 2076–2088. [[CrossRef](#)] [[PubMed](#)]
46. Fischer, A.N.M.; Fuchs, E.; Mikula, M.; Huber, H.; Beug, H.; Mikulits, W. PDGF essentially links TGF- β signaling to nuclear β -catenin accumulation in hepatocellular carcinoma progression. *Oncogene* **2007**, *26*, 3395–3405. [[CrossRef](#)] [[PubMed](#)]
47. Kong, D.; Wang, Z.; Sarkar, S.H.; Li, Y.; Banerjee, S.; Saliganan, A.; Kim, H.R.C.; Cher, M.L.; Sarkar, F.H. Platelet-Derived Growth Factor-D Overexpression Contributes to Epithelial-Mesenchymal Transition of PC3 Prostate Cancer Cells. *Stem Cells* **2008**, *26*, 1425–1435. [[CrossRef](#)]
48. Baumann, K.H.; du Bois, A.; Meier, W.; Rau, J.; Wimberger, P.; Sehouli, J.; Kurzeder, C.; Hilpert, F.; Hasenburger, A.; Canzler, U.; et al. A phase II trial (AGO 2.11) in platinum-resistant ovarian cancer: A randomized multicenter trial with sunitinib (SU11248) to evaluate dosage, schedule, tolerability, toxicity and effectiveness of a multitargeted receptor tyrosine kinase inhibitor monotherapy. *Ann. Oncol. Off. J. Eur. Soc. Med. Oncol.* **2012**, *23*, 2265–2271. [[CrossRef](#)]
49. Biagi, J.J.; Oza, A.M.; Chalchal, H.I.; Grimshaw, R.; Ellard, S.L.; Lee, U.; Hirte, H.; Sederias, J.; Ivy, S.P.; Eisenhauer, E.A. A phase II study of sunitinib in patients with recurrent epithelial ovarian and primary peritoneal carcinoma: An NCIC Clinical Trials Group Study. *Ann. Oncol. Off. J. Eur. Soc. Med. Oncol.* **2011**, *22*, 335–340. [[CrossRef](#)]
50. Cazet, A.S.; Hui, M.N.; Elsworth, B.L.; Wu, S.Z.; Roden, D.; Chan, C.L.; Skhinas, J.N.; Collot, R.; Yang, J.; Harvey, K.; et al. Targeting stromal remodeling and cancer stem cell plasticity overcomes chemoresistance in triple negative breast cancer. *Nat. Commun.* **2018**, *9*, 2897. [[CrossRef](#)]
51. Ito, T.; Tori, M.; Hashigaki, S.; Kimura, N.; Sato, K.; Ohki, E.; Sawaki, A.; Okusaka, T. Efficacy and safety of sunitinib in Japanese patients with progressive, advanced/metastatic, well-differentiated, unresectable pancreatic neuroendocrine tumors: Final analyses from a Phase II study. *Jpn. J. Clin. Oncol.* **2019**, *49*, 354–360. [[CrossRef](#)] [[PubMed](#)]
52. Raymond, E.; Kulke, M.H.; Qin, S.; Yu, X.; Schenker, M.; Cubillo, A.; Lou, W.; Tomasek, J.; Thiis-Evensen, E.; Xu, J.M.; et al. Efficacy and Safety of Sunitinib in Patients with Well-Differentiated Pancreatic Neuroendocrine Tumours. *Neuroendocrinology* **2018**, *107*, 237–245. [[CrossRef](#)] [[PubMed](#)]
53. Roskoski, R. The role of small molecule platelet-derived growth factor receptor (PDGFR) inhibitors in the treatment of neoplastic disorders. *Pharmacol. Res.* **2018**, *129*, 65–83. [[CrossRef](#)]
54. Stathis, A.; Hess, D.; von Moos, R.; Homicsko, K.; Griguolo, G.; Joerger, M.; Mark, M.; Ackermann, C.J.; Allegrini, S.; Catapano, C.V.; et al. Phase I trial of the oral smoothened inhibitor sonidegib in combination with paclitaxel in patients with advanced solid tumors. *Investig. New Drugs* **2017**, *35*, 766–772. [[CrossRef](#)] [[PubMed](#)]
55. Bregenzer, M.E.; Davis, C.; Horst, E.N.; Mehta, P.; Novak, C.M.; Raghavan, S.; Snyder, C.S.; Mehta, G. Physiologic Patient Derived 3D Spheroids for Anti-neoplastic Drug Screening to Target Cancer Stem Cells. *J. Vis. Exp.* **2019**. [[CrossRef](#)] [[PubMed](#)]

56. Mehta, P.; Novak, C.; Raghavan, S.; Ward, M.; Mehta, G. Self-Renewal and CSCs In Vitro Enrichment: Growth as Floating Spheres. In *Cancer Stem Cells: Methods and Protocols*; Papaccio, G., Desiderio, V., Eds.; Springer: New York, NY, USA, 2018; pp. 61–75.
57. Raghavan, S.; Mehta, P.; Horst, E.N.; Ward, M.R.; Rowley, K.R.; Mehta, G. Comparative analysis of tumor spheroid generation techniques for differential in vitro drug toxicity. *Oncotarget* **2016**. [[CrossRef](#)]
58. Raghavan, S.; Ward, M.R.; Rowley, K.R.; Wold, R.M.; Takayama, S.; Buckanovich, R.J.; Mehta, G. Formation of stable small cell number three-dimensional ovarian cancer spheroids using hanging drop arrays for preclinical drug sensitivity assays. *Gynecol. Oncol.* **2015**, *138*, 181–189. [[CrossRef](#)]
59. Charafe-Jauffret, E.; Ginestier, C.; Iovino, F.; Tarpin, C.; Diebel, M.; Esterni, B.; Houvenaeghel, G.; Extra, J.M.; Bertucci, F.; Jacquemier, J.; et al. Aldehyde Dehydrogenase 1-Positive Cancer Stem Cells Mediate Metastasis and Poor Clinical Outcome in Inflammatory Breast Cancer. *Clin. Cancer Res.* **2010**, *16*, 45–55. [[CrossRef](#)]
60. Neri, S.; Miyashita, T.; Hashimoto, H.; Suda, Y.; Ishibashi, M.; Kii, H.; Watanabe, H.; Kuwata, T.; Tsuboi, M.; Goto, K.; et al. Fibroblast-led cancer cell invasion is activated by epithelial-mesenchymal transition through platelet-derived growth factor BB secretion of lung adenocarcinoma. *Cancer Lett.* **2017**, *395*, 20–30. [[CrossRef](#)]
61. Steller, E.J.; Raats, D.A.; Koster, J.; Rutten, B.; Govaert, K.M.; Emmink, B.L.; Snoeren, N.; van Hooff, S.R.; Holstege, F.C.; Maas, C.; et al. PDGFRB promotes liver metastasis formation of mesenchymal-like colorectal tumor cells. *Neoplasia* **2013**, *15*, 204–217. [[CrossRef](#)]
62. Roodhart, J.M.L.; Daenen, L.G.M.; Stigter, E.C.A.; Prins, H.J.; Gerrits, J.; Houthuijzen, J.M.; Gerritsen, M.G.; Schipper, H.S.; Backer, M.J.G.; van Amersfoort, M.; et al. Mesenchymal Stem Cells Induce Resistance to Chemotherapy through the Release of Platinum-Induced Fatty Acids. *Cancer Cell* **2011**, *20*, 370–383. [[CrossRef](#)] [[PubMed](#)]
63. Melaiu, O.; Catalano, C.; De Santi, C.; Cipollini, M.; Figlioli, G.; Pellè, L.; Barone, E.; Evangelista, M.; Guazzelli, A.; Boldrini, L.; et al. Inhibition of the platelet-derived growth factor receptor beta (PDGFRB) using gene silencing, crenolanib besylate, or imatinib mesylate hampers the malignant phenotype of mesothelioma cell lines. *Genes Cancer* **2017**, *8*, 438–452. [[CrossRef](#)] [[PubMed](#)]
64. Shih, A.H.; Holland, E.C. Platelet-derived growth factor (PDGF) and glial tumorigenesis. *Cancer Lett.* **2006**, *232*, 139–147. [[CrossRef](#)]
65. Tsao, A.S.; Wei, W.; Kuhn, E.; Spencer, L.; Solis, L.M.; Suraokar, M.; Lee, J.J.; Hong, W.K.; Wistuba, I.I. Immunohistochemical overexpression of platelet-derived growth factor receptor-beta (PDGFR- β) is associated with PDGFRB gene copy number gain in sarcomatoid non-small cell lung cancer (NSCLC). *Clin. Lung Cancer* **2011**, *12*, 369–374. [[CrossRef](#)] [[PubMed](#)]
66. Matei, D.; Emerson, R.E.; Lai, Y.C.; Baldrige, L.A.; Rao, J.; Yiannoutsos, C.; Donner, D.D. Autocrine activation of PDGFR α promotes the progression of ovarian cancer. *Oncogene* **2006**, *25*, 2060. [[CrossRef](#)]
67. Juliachs, M.; Muñoz, C.; Moutinho, C.A.; Vidal, A.; Condom, E.; Esteller, M.; Graupera, M.; Casanovas, O.; Germà, J.R.; Villanueva, A.; et al. The PDGFR β -AKT Pathway Contributes to CDDP-Acquired Resistance in Testicular Germ Cell Tumors. *Clin. Cancer Res.* **2014**, *20*, 658–667. [[CrossRef](#)]
68. Li, X.; Ma, Q.; Xu, Q.; Liu, H.; Lei, J.; Duan, W.; Bhat, K.; Wang, F.; Wu, E.; Wang, Z. SDF-1/CXCR4 signaling induces pancreatic cancer cell invasion and epithelial-mesenchymal transition in vitro through non-canonical activation of Hedgehog pathway. *Cancer Lett.* **2012**, *322*, 169–176. [[CrossRef](#)] [[PubMed](#)]
69. Wu, Q.; Hou, X.; Xia, J.; Qian, X.; Miele, L.; Sarkar, F.H.; Wang, Z. Emerging roles of PDGF-D in EMT progression during tumorigenesis. *Cancer Treat. Rev.* **2013**, *39*, 640–646. [[CrossRef](#)]
70. Levanat, S.; Sabol, M.; Musani, V.; Ozretic, P.; Trnski, D. Hedgehog Signaling Pathway as Genetic and Epigenetic Target in Ovarian Tumors. *Curr. Pharm. Des.* **2017**, *23*, 73–94. [[CrossRef](#)]
71. Song, X.; Yan, L.; Lu, C.; Zhang, C.; Zhu, F.; Yang, J.; Jing, H.; Zhang, Y.; Qiao, J.; Guo, H. Activation of hedgehog signaling and its association with cisplatin resistance in ovarian epithelial tumors. *Oncol. Lett.* **2018**, *15*, 5569–5576. [[CrossRef](#)]
72. Liao, X.; Siu, M.K.Y.; Au, C.W.H.; Wong, E.S.Y.; Chan, H.Y.; Ip, P.P.C.; Ngan, H.Y.S.; Cheung, A.N.Y. Aberrant activation of hedgehog signaling pathway in ovarian cancers: Effect on prognosis, cell invasion and differentiation. *Carcinogenesis* **2009**, *30*, 131–140. [[CrossRef](#)] [[PubMed](#)]
73. Becher, O.J.; Hambarzumyan, D.; Fomchenko, E.I.; Momota, H.; Mainwaring, L.; Bleau, A.M.; Katz, A.M.; Edgar, M.; Kenney, A.M.; Cordon-Cardo, C.; et al. Gli Activity Correlates with Tumor Grade in Platelet-Derived Growth Factor-Induced Gliomas. *Cancer Res.* **2008**, *68*, 2241–2249. [[CrossRef](#)] [[PubMed](#)]

74. Charles, N.; Ozawa, T.; Squatrito, M.; Bleau, A.M.; Brennan, C.W.; Hambardzumyan, D.; Holland, E.C. Perivascular Nitric Oxide Activates Notch Signaling and Promotes Stem-like Character in PDGF-induced Glioma Cells. *Cell Stem Cell* **2010**, *6*. [[CrossRef](#)]
75. Yao, Q.; Renault, M.A.; Chapouly, C.; Vandierdonck, S.; Belloc, I.; Jaspard-Vinassa, B.; Daniel-Lamazière, J.M.; Laffargue, M.; Merched, A.; Desgranges, C.; et al. Sonic hedgehog mediates a novel pathway of PDGF-BB-dependent vessel maturation. *Blood* **2014**, *123*, 2429–2437. [[CrossRef](#)]



© 2020 by the authors. Licensee MDPI, Basel, Switzerland. This article is an open access article distributed under the terms and conditions of the Creative Commons Attribution (CC BY) license (<http://creativecommons.org/licenses/by/4.0/>).